The high overtone and combination levels of SF6 revisited at Doppler-limited resolution: A global effective rovibrational model for highly excited vibrational states

M. Faye, V. Boudon, M. Loëte, Pascal Roy, L. Manceron

Journal of xxxxxxxxxxx, Vol. 00, No. 00, DD Month 2016, 1–13

The high overtone and combination levels of SF_6 revisited at Doppler-limited resolution: a global effective rovibrational model for highly excited vibrational states

M. Faye[a], V. Boudon[b]*, M. Loëte[b], P. Roy[a], L. Manceron[a,c]*.

[a] *Ligne AILES–Synchrotron SOLEIL, L'Orme des Merisiers, F-91192 Gif-sur-Yvette, France,*
[b] *Laboratoire Interdisciplinaire Carnot de Bourgogne, UMR 6303 CNRS-Université de Bourgogne Franche-Comté 9 Av. A. Savary, BP 47870, F-21078 Dijon Cedex, France,*
[c] *Laboratoire MONARIS, CNRS UMR 8233, 4 Place Jussieu, F-75252 Paris Cedex, France,*

(*Received 00 Month 200x; In final form 00 Month 200x*)

Sulfur hexafluoride is an important prototypal molecule for modeling highly excited vibrational energy flow and multi quanta absorption processes in hexafluoride molecules of technological importance. It is also a strong greenhouse gas of anthropogenic origin. This heavy species, however, features many hot bands at room temperature (at which only 30 % of the molecules lie in the ground vibrational state), especially those originating from the lowest, v_6=1 vibrational state. Using a cryogenic long path cell with variable optical path length and temperatures regulated between 120 and 163K , coupled to Synchrotron Radiation and a high resolution interferometer, Doppler-limited spectra of the $2\nu_1+\nu_3$, $\nu_1+\nu_2+\nu_3$, $\nu_1+\nu_3$, $\nu_2+\nu_3$, $3\nu_3$, $\nu_2+3\nu_3$ and $\nu_1+3\nu_3$ from 2000 to 4000 cm-1 near-infrared region has been recorded. Low temperature was used to limit the presence of hot bands. The spectrum has been analyzed thanks to the XTDS software package. Combining with previously observed weak difference bands in the far infrared region involving the v_1, v_2, v_3=1 states, we are thus able to use the tensorial model to build a global fit of spectroscopic parameters for v_1=1,2, v_2=1, v_3=1,2,3. The model constitutes a consistent set of molecular parameters and enable spectral rovibrational simulation for all multi-quanta transitions involving v_1, v_2 and v_3 up to v_{1-3}=3. Tests simulation on rovibrational transitions not yet rovibrationally assigned are presented and compared to new experimental data.

Keywords: Rotation-vibration spectroscopy of SF_6, greenhouse gas, hot band, infrared absorption, tensorial formalism, Long path cell, low temperature

1 Introduction

Sulfur hexafluoride (SF_6), an octahedral molecule of O_h symmetry, is of fundamental interest in several aspects. In particular, it is a test case for the complex molecular spectroscopy of hexafluoride molecules of well-known technological importance [1, 2]. This has motivated a great deal of work on multi quanta absorption using powerful IR lasers [3] on the mechanisms involved in vibrational energy relaxations [4]. Explaining the initial isotope-selective stages of multiple-photon dissociation using high power IR lasers has motivated earlier studies of the ν_3 vibrational manifold to model the complex anharmonic effects encountered in these highly symmetric molecules. A remarkable effort was made in this direction by Pine and Robiette [5] and Patterson, Crown and Pine [6] observing the $3\nu_3$ manifold between 2819 and 2832 cm^{-1} at high resolution using a tunable laser difference-frequency spectrometer. They could analyze a good part of the $3\nu_3$ manifold absorption spectrum as an isolated band while taking into account the interaction between l=1 and 3 sub-bands. This analysis built up on the previously available knowledge of the ν_3 band but could not fit in a more comprehensive analysis between all levels involving several quanta of v_1, v_2 and v_3, which may be significant for laser-driven isotopically selective separation processes. Since then, further studies have led to a more global effective Hamiltonian, of larger predictive power. The infrared spectrum of gaseous SF_6 has been extensively studied at low resolution [8] and therein and all its fundamentals have been observed at high to very high resolution and analyzed in detail [9, 16]. Furthermore, SF_6 is a strong greenhouse gas with a very long life time in the stratosphere ($\simeq$ 23900 years). Being an important Earth

* Corresponding authors
E-mail adress1: Vincent.Boudon@u-bourgogne.fr E-mail adress2: laurent.manceron@synchrotron-soleil.fr

atmospheric pollution marker. The relevance of IR spectroscopy for the quantification of SF_6 in the upper atmosphere has renewed the interest for its study [17].

The six fundamentals of SF_6 can be divided in three stretching motions, ν_1 to ν_3, of A_{1g}, E_g and F_{1u} symmetry and three bending modes, ν_4 to ν_6, of F_{1u}, F_{2g} and F_{2u} symmetry. As ν_3 and ν_4 have the same symmetry, only these two modes can present mixtures of stretching and bending coordinates at first order. Other effects such as high order Coriolis couplings can induce mixture with the IR inactive F_{2u} mode, but all these effects have been shown to be small [16, 19]. At present, with the progress in laser technology in the near IR and UV, it will become conceivable to induce isotopically selective two-photon ionization/dissociation scheme. Thus, precise rovibrational spectroscopy for highly excited vibrational levels involving several quanta of stretching modes may become important. Past efforts in this direction have used FTIR absorption spectroscopy at moderated resolution high pressure × optical path length sample [20, 21] next, photoacoustic spectroscopy with tunable lasers. Levene and Perry have used a broadly tunable OPO to investigate quaternary combinations of the stretching modes and fitted the assigned transitions with an effective model to derive anharmonic splitting constants [22]. This effort was accompanied by theoretical developments to explicit relations between quadratic and higher order potential terms and vibrational anharmonic coefficients for octahedral molecules [22, 24] and led to important predictions of anharmonic coefficients (X_{ij}, G_{ij}, T_{ij} in the notation of Hecht [25]). Later, Zhang *et al.* used the same technique to investigate other, weaker ternary combinations and overtone of SF_6 and UF_6 with a CO laser [26]. These studies were, however, limited by the laser resolution and pressure broadening effects to observation of unresolved rotational contours. Using the newly developed instrumentation at Synchrotron SOLEIL (France), involving synchrotron radiation [27, 28], a cryogenic long path cell [29] and high sensitivity detectors [30], rotationally resolved spectra could be acquired for such very weak transitions (band intensities of ca 0.02 to 0.0005 km/mole) and are presented here. In this study we increase the level of our previous effective global model [31] to take into account the $3\nu_3$ band in full, as well as new data on ν_3, $\nu_1+\nu_3$, $\nu_2+\nu_3$, $\nu_1+\nu_2+\nu_3$ and $3\nu_3$ transitions. This is combined with previously acquired data on $\nu_3-\nu_2$, $\nu_3-\nu_1$ [31], $2\nu_3$ [32, 33], $2\nu_3-\nu_3$ bands and Raman active fundamentals ν_1 and ν_2 Ref. [13, 15]. Our present goal is thus now to provide a model and a consistent effective parameter set enabling to recalculate with its rotational structure, any vibrational band with stretching mode quantum numbers v_1, v_2=1,2 and v_3=1,2,3.

2 Theoretical model

The theoretical model used here is based on the cubic tensor formalism and the vibrational extrapolation developed by the Dijon group [10]. We simply recall the principles here. Considering an XY_6 molecule as SF_6, the vibrational levels are grouped in series of polyads called P_k with $k=0,...,n$. For $k=0$, we have P_0 which is the ground state (GS). The Hamiltonian operator is thus written as follow:

$$\mathcal{H}=\mathcal{H}_{\{P_0\equiv GS\}}+\mathcal{H}_{\{P_1\}}+\ldots+\mathcal{H}_{\{P_k\}}+\ldots+\mathcal{H}_{\{P_{n-1}\}}+\mathcal{H}_{\{P_n\}}. \quad (1)$$

where the different $\mathcal{H}_{\{P_k\}}$ terms which contain the rovibrational operators are expressed in the following form:

$$\mathcal{H}_{\{P_k\}}=\sum_{\text{all indexes}} t^{\Omega(K,n\Gamma)\Gamma_v\Gamma'_v}_{\{s\}\{s'\}}\beta\left[{}^{\varepsilon}V^{\Omega_v(\Gamma_v\Gamma'_v)\Gamma}_{\{s\}\{s'\}}\otimes R^{\Omega(K,n\Gamma)}\right]^{(A_{1g})}. \quad (2)$$

In this equation (2), the $t^{\Omega(K,n\Gamma)\Gamma v\Gamma' v}$ are the parameters to be determined, while ${}^{\varepsilon}V^{\Omega_v(\Gamma_v\Gamma'_v)\Gamma}_{\{s\}\{s'\}}$ and $R^{\Omega(K,n\Gamma)}$ are vibrational and rotational operators, respectively, and of respective degree Ωv and Ω. β is a factor that allows the scalar terms ($\Gamma=A_{1g}$) to match the usual terms like B_0J^2, etc. To generalize, we have:

$$\beta = \begin{cases} \sqrt{3}(\sqrt{3}/4)^{\Omega/2} \text{ if } (K, n\Gamma) = (0, 0A_{1g}) \\ 1 \quad \text{Otherwise} \end{cases}.$$

The order of each individual term is defined as $\Omega + \Omega_v - 2$.

In this model we deal with an effective Hamiltonian which is obtained, for a given polyad P_k, by the projection of H in the P_n Hilbert subspace; see equation (3).

$$\begin{aligned} H^{<P_n>} &= P^{<P_n>} \mathcal{H} P^{<P_n>} \\ &= H^{<P_n>}_{\{\mathrm{GS}\}} + H^{<P_n>}_{\{P_1\}} + \ldots + H^{<P_n>}_{\{P_k\}} + \ldots + H^{<P_n>}_{\{P_{n-1}\}} + H^{<P_n>}_{\{P_n\}}. \end{aligned} \tag{3}$$

This Hamiltonian expression allow the systematic treatment of any polyad system.

The calculation of the effective Hamiltonian matrix was performed in the coupled rovibrational basis

$$\left| \left[\Psi_v^{(C_v)} \otimes \Psi_r^{(J,nC_r)} \right]^{(C)} \right\rangle, \tag{4}$$

where $\Psi_r^{(J,nC_r)}$ is a rotational wavefunction with angular momentum J, rotational symmetry species C_r and multiplicity index n and C the overall symmetry species ($C = C_v \otimes C_r$). The effective dipole moment operator, used to calculate transition intensities is expanded in a similar way. It is expanded here up to order 2 (see below) and its matrix elements are calculated in the Hamiltonian's eigenbasis set.

3 Experimental

Because of the weakness of the difference bands or multi quanta transitions combined with the presence of hot bands at room temperature, a long optical path length at low temperature was required. In the far- and mid-IR, several high resolution spectra were recorded on the AILES Beamline on the synchrotron light source SOLEIL coupled to the Bruker 125HR interferometer [27, 28] using the newly developed cryogenic long path cell regulated at temperature between 125 and 153K along the entire optical path. This setup has been fully described elsewhere [29]. In the near IR (> 2000 cm-1) a quartz halogen lamp was used as a source. A spectrum with a gas pressure of 4.5 mbar of SF_6 (Air Liquide, France, 99.99% purity) was recorded at 0.002 cm^{-1} resolution in the 600-80 cm-1 region, using boxcar apodization, 5.06 cm/s scanner velocity, a 6 μm Si/Mylar beamsplitter and a 4 K-cooled Si composite bolometer with a 1.5 ms rise time and a cold, 600 cm^{-1} low-pass filter. 576 interferograms were averaged in a total recording time of about 38 hours and processed against a background of the empty cell taken at the same 163 K temperature at 0.01 cm^{-1} resolution. Spectra in the mid IR range were acquired at 0.002 cm^{-1} resolution using a KBr/Ge beamsplitter and a home-made high sensitivity HgCdTe detector [30] using path lengths varied between 15 and 93 m. Spectra in the near infrared region were taken between 2000 and 4000 cm^{-1} with an InSb detector, using 93 and 27 m optical path length with 5 and 1.5 mbar sample pressure, respectively. For these measurements, the diamond cell outer windows used for the MIR/ FIR were replaced by from diamond to AR-coated ZnSe, improving the optical throughput by a factor of 1.9. Spectra were zero-filled, corrected for channelling effects and calibrated using well-known water, carbon dioxide or carbonyl sulphide rotational lines [34].

4 Global strategy for the simultaneous fit of SF_6 data

In this work, we gather data from both infrared and Raman measurements to achieve a global fit of the ensemble of ν_1, ν_2, ν_3, $\nu_1 + \nu_3$, $\nu_2 + \nu_3$, $2\nu_3$, $2\nu_3 - \nu_3$, $\nu_1 + \nu_2 + \nu_3$, $3\nu_3$, $\nu_3 - \nu_1$ and $\nu_3 - \nu_2$ bands of SF_6.

The ν_1 and ν_2 data obtained from Raman measurements in Refs. [13, 15] and $2\nu_3$, $2\nu_3 - \nu_3$ obtained by double resonance technique are derived from Ref. [35]. The $\nu_3 - \nu_1$ and $\nu_3 - \nu_2$ data were also given in Ref. [31]. For ν_3, $\nu_1 + \nu_3$, $\nu_2 + \nu_3$, $\nu_1 + \nu_2 + \nu_3$, $3\nu_3$ bands, we found that it was possible to improve

notably the measurements precision using the SOLEIL synchrotron setup. So, high resolution analyses of the bands are shown in the sections below. In order to access the anharmonicity implying the v_1=v_2=1 state, we also measured the $\nu_1+\nu_2+\nu_3$ ternary combination band. The global fit of all these data provides a consistent set of parameters allowing to predict a large number of other transitions implying the ν_1, ν_2 and ν_3 fundamental modes of SF_6. As a test of efficiency of the predictive power of this model, we present in the last section, predictions of $\nu_1+3\nu_3$ and $\nu_2+3\nu_3$ bands and new measurements of the ternary transitions at the Doppler-limited resolution.

5 The ν_3 band

The ν_3 band of SF_6 has been the object of many studies (see Refs. [8, 9] and therein). These investigations were performed using CO_2 laser absorption spectroscopy method with a very high precision, but these concerned transitions with low J values. In the course of the present study, while revisiting the ν_3 data, even at our resolution, we noticed that the available parameters did not allow a completely satisfactory simulation of the entire ν_3 band, especially for high J value transitions. A new spectrum in the ν_3 region was recorded using the SOLEIL synchrotron source and the cryogenic multi pass cell with 69 m of optical path. SF_6 was diluted with N_2 in order to obtain very low partial pressures of SF_6 and record spectra near 125 K with virtually no hot bands. Table 1 summarizes the different conditions of recording the spectrum. By using the parameters of Ref. [11] to calculate the spectrum, we found a good agreement between the simulation and the experiment for low J values ($J \leq 33$). For higher J in both P and R branches ($J \geq 33$) however, the line positions were getting further to the experiment and the standard deviation was found to be up to 0.005 cm^{-1}. It was thus required to achieve a new fit to improve the Hamiltonian parameters. Fig. 1 shows the simulated (in red) and experimental (in blue) spectrum of the ν_3 band. The fit residuals are shown by black markers at the bottom of the figure. The standard deviation now appears to be of the order of 0.003 cm^{-1}.

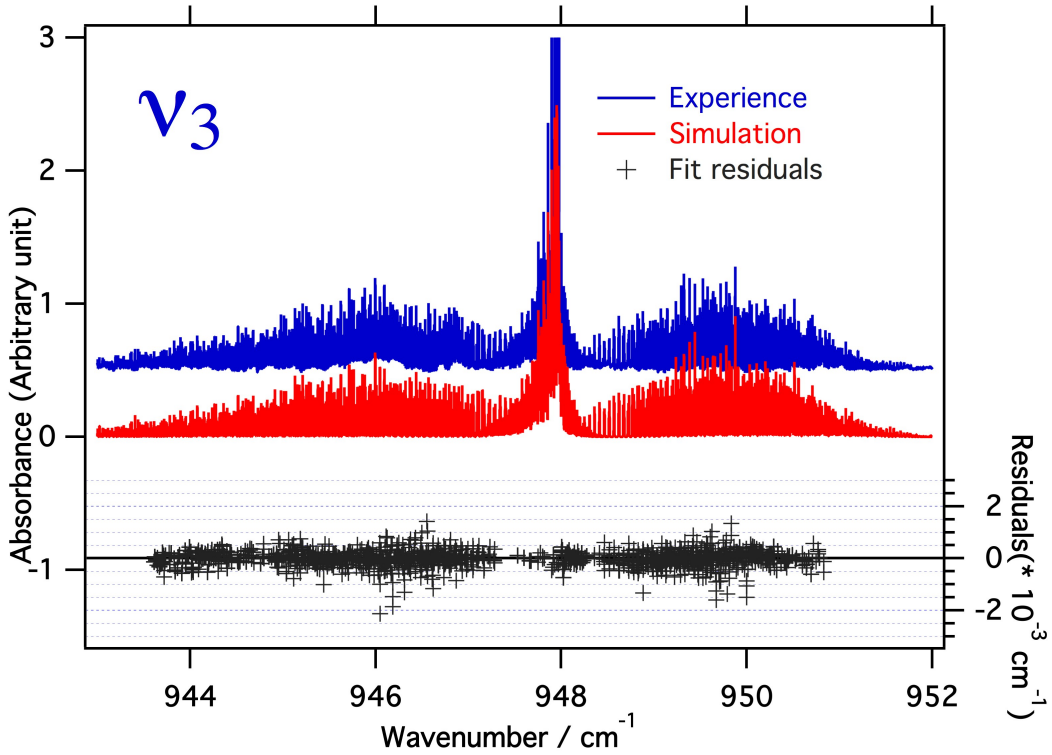

Figure 1. Comparison between the simulation(red) and the experiment (blue) spectrum recorded over the whole ν_3 band, showing the agreement achieved. It should be noticed that the strong Q branch is saturated in the experimental spectrum.

Table 1. Summary of the four different conditions of measurement of ν_3 .

Conditions	P(N_2+SF_6)(mbar)	P(SF_6)(mbar)	OPL(cm)	T(K)	Resolution (cm^{-1})
Condition 1	1.15	1.24×10^{-5}	6900	138	0.002
Condition 2	1.16	2.42×10^{-5}	6900	125	0.002
Condition 3	1.16	3.53×10^{-5}	6900	125	0.002
Condition 4	1.16	3.53×10^{-5}	6900	173	0.002

OPL: Optical Path Length
P(SF_6): Partial pressure of SF_6
P(N_2+SF_6): Total Pressure of N_2+SF_6
T: Temperature

6 The $\nu_1+\nu_3$ and $\nu_2+\nu_3$ bands

The $\nu_1+\nu_3$ and $\nu_2+\nu_3$ SF_6 bands had previously been recorded at very low temperature, 25 K, thanks to a molecular supersonic jet technique; the Jet-AILES setup [31]. At that low temperature the structure of spectrum was very simplified but the resolution was limited to 0.005 cm^{-1}. In this study 444 rovibrational lines were assigned and fitted for $\nu_2+\nu_3$ and 123 for $\nu_1+\nu_3$. The main goal of this study was to refine the anharmonicity constants X_{31} and X_{32} in order to calculate their corresponding hot bands $\nu_1+\nu_3-\nu_1$ and $\nu_2+\nu_3-\nu_2$.

In a first attempt at a global fit, it was found, however, that the deviation between observed and calculated lines was greater in this series. To improve the analysis for these two bands, we performed new infrared absorption measurements in this region, using the cryogenic multi-pass cell. For these measurements, we used a SF_6 sample cooled down to 153 K, at 0.14 mb of pressure and we set the optical path to 15 m. Under these conditions, we could double the resolution to 0.0025 cm^{-1} and increase largely the number of observed transitions.

By using the HTDS program, based on a tensorial formalism of the Hamiltonian, we performed new analyses of both $\nu_1+\nu_3$ and $\nu_2+\nu_3$ bands. For each band, the Hamiltonian is developed up to the sixth order. The maximum value of the rotational quantum number J_{max} is equal to 63 and 72 for $\nu_1+\nu_3$ and $\nu_2+\nu_3$ respectively. For the two bands, we have now increased significantly the number of assignments. For $\nu_1+\nu_3$ we assigned and fit 1163 line positions, versus 123 in the previous study, with a standard deviation down to 0.279×10^{-3} cm^{-1}. The X_{13} anharmonicity constant is determined to be $-2.90888(8)$ cm^{-1} with improved accuracy with respect to the previous determinations ($-2.902(3)$ cm^{-1} in Ref. [21], $-2.9088(2)cm^{-1}$ in Ref. [31]) and the prediction -2.94 cm^{-1} [24]. For $\nu_2+\nu_3$ we assigned and fitted 3256 line positions versus 444 in the previous study, with a standard deviation of 0.450×10^{-3} cm^{-1}. Because of the two sub-levels F_{1u} and F_{2u} of this band, the anharmonicity constants should be given by the expressions $X_{23}+G_{22}+8T_{23}$ for F_{1u} and $X_{23}+G_{22}-8T_{23}$ for F_{2u}. But due to the lack of knowledge for $2\nu_2$, we have no value for G_{22}. We could nevertheless derive the T_{23} constant from the energies of the sub-levels ($F_{1u}\longrightarrow 1587.717292$ cm^{-1}, $F_{2u}\longrightarrow 1591.192261$ cm^{-1}) and thus T_{23}=-0.2172 cm^{-1}, which compares favorably with the prediction of -0.213 [24]. Fig. 2 and Fig. 3 show the result of the analysis of $\nu_1+\nu_3$ and $\nu_2+\nu_3$ respectively illustrating the agreement between the experiment in blue color and the simulation in red color. At the bottom of each figures, we also show the fit residuals of the line assignments.

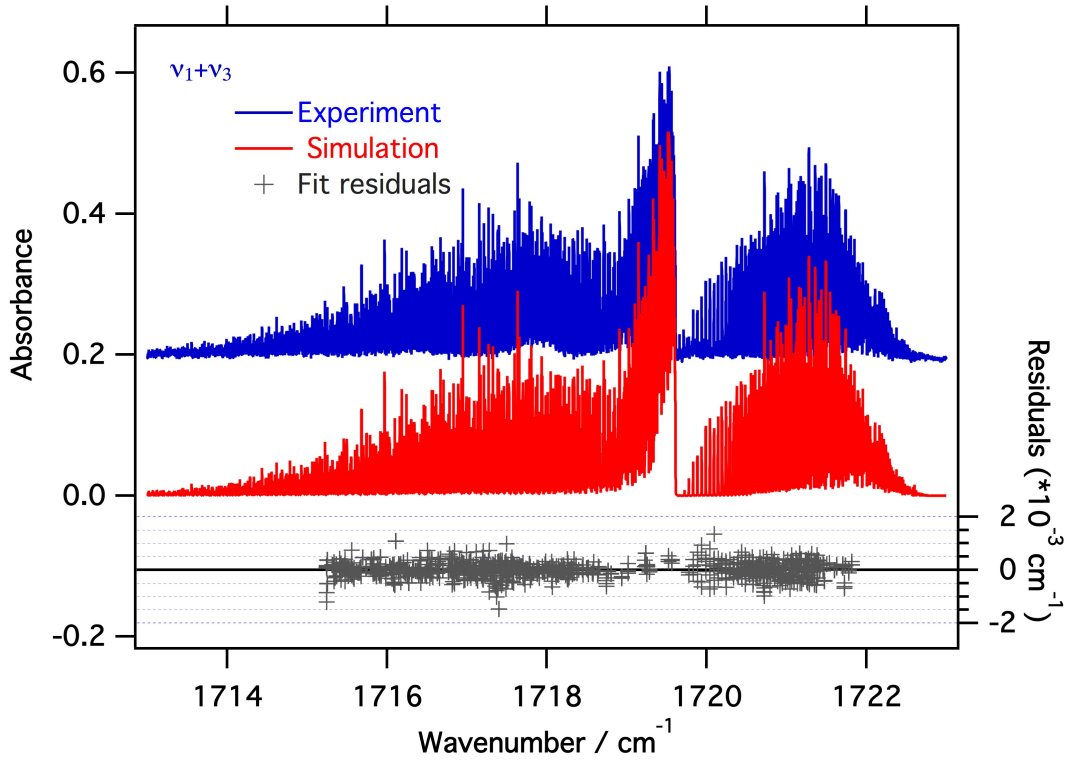

Figure 2. Comparison between the simulation (red) and the experiment (blue) spectra recorded over the whole $\nu_1 + \nu_3$ band.

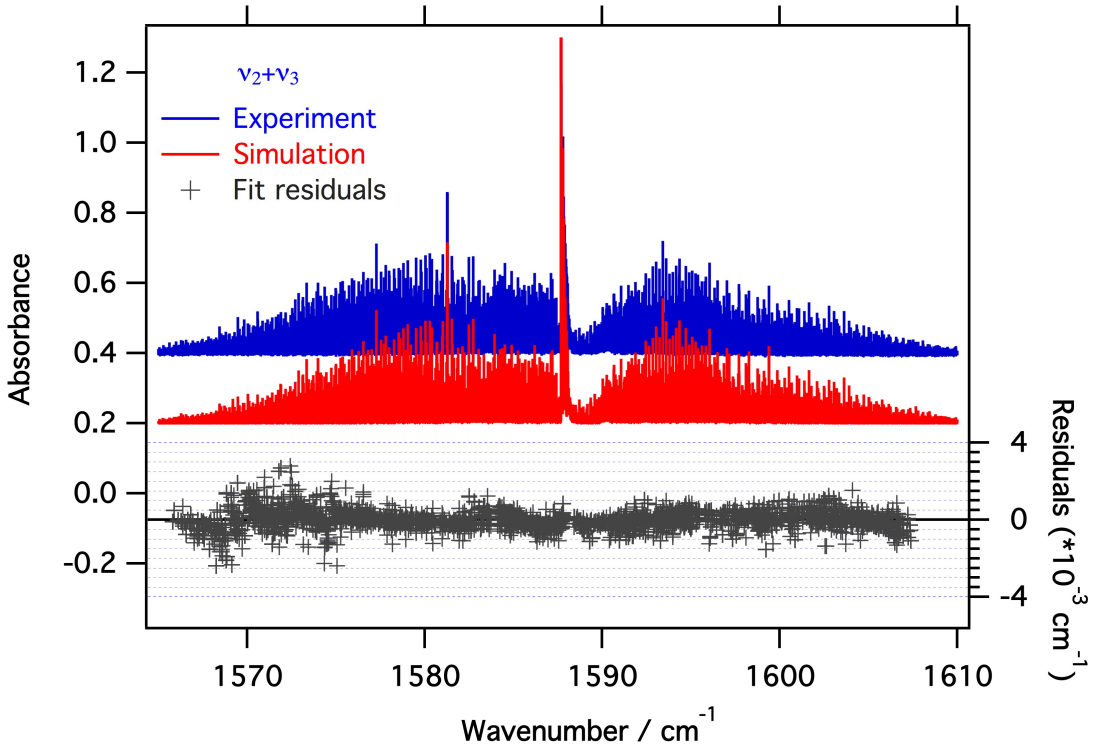

Figure 3. Comparison between the simulation (red) and the experiment (blue) spectra recorded over the whole $\nu_1 + \nu_3$ band.

7 The $\nu_1 + \nu_2 + \nu_3$ band

By considering the symmetry species A_{1g}, E_g and F_{1u} of the ν_1, ν_2 and ν_3 modes respectively, the direct product gives $A_{1g} \bigotimes E_g \bigotimes F_{1u} \longrightarrow E_g \bigotimes F_{1u} \longrightarrow F_{1u} \bigoplus F_{2u}$. Thus, the $\nu_1+\nu_2+\nu_3$ band has two sub-levels F_{1u} and F_{2u}. In the infrared absorption spectrum only the F_{1u} component arises and gives a relatively simple structure to analyze. The simulation was performed by developing the Hamiltonian to the 6^{th} order. We assigned line positions up to J_{max}=90 and fitted 2856 transitions with 21 parameters. Fig. 4 shows the experiment vs simulation spectra for this band and the fit residuals the bottom of the figure. The standard deviation is here equal to 0.860×10^{-3} cm^{-1}. The analysis of $\nu_1 + \nu_2 + \nu_3$ band allows to a simultaneous access of ν_1, ν_2 and ν_3 parameters and also to the anharmonicity constant X_{12} of the $\nu_1 + \nu_2$ band which is not active in infrared because of its E_g symmetry. This anharmonicity constant is found to be $X_{12} = -2.4816(3)$ cm^{-1}, which compares very well to the -2.49 cm^{-1} prediction of Ref. [24], and not as favorably the $-2.37(1)$ cm^{-1} previous estimate [20].

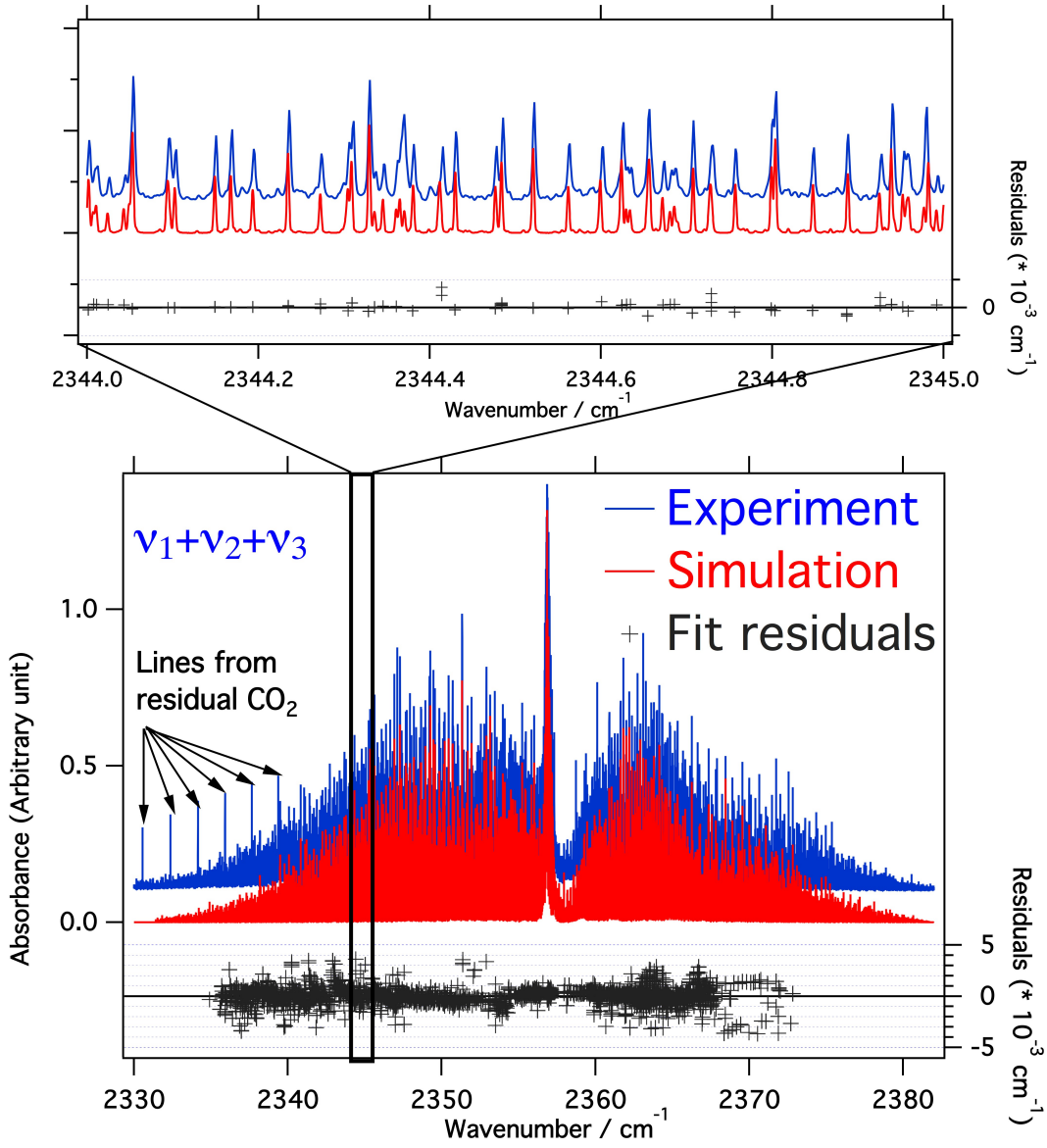

Figure 4. The $\nu_1 + \nu_2 + \nu_3$ band, Experiment in blue vs simulation in red with a zoom in the P branch, showing the good agreement of the fit.

8 Study on the $3\nu_3$ band

The $2\nu_3$ band is of g symmetry (with A_{1g}, E_g, F_{2g} sublevels), and is therefore forbidden for infrared direct one-photon absorption. A study of this band using Doppler Free Two-Photon spectroscopy is reported in [7]. The $3\nu_3$ band is of u symmetry (with A_{2u}, F_{2u}, $2F_{1u}$ sublevels), and is infrared active. It is therefore the most direct way to access the X_{33}, G_{33} and T_{33} anharmonic constants that determine the $n\nu_3$ ladder, see Equation (5). This band has thus been the object of several previous analyses by A. S. Pine *et al* [5, 6]. In both studies they used the same experimental setup: a tunable laser difference-frequency spectrometer coupled to a White cell. In the first study, the authors performed the analysis by focusing only on one F_{1u} sub-level (with essentially $l = 1$ character). While their second investigation presents an analysis using a perturbed Hamiltonian model which takes into account the $l = 1$ character and the interaction between the sub-levels [6]. This last study brought a more complete understanding of the structure of the $3\nu_3$ band. In these previous studies, however, the maximum number of lines assigned and fitted was only around 700 with $J_{max} \leq 33$.

In this paper, we present a new analysis of the band using a spectrum recorded at the SOLEIL Synchrotron with a resolution of 0.0025 cm^{-1}, thanks to the multi pass cell coupled to a high resolution Fourier Transform spectrometer. We could extend the assignment up to 3759 lines with J_{max}=77 far more complete than the previous assignement [6] with an improved standard deviation of $1.157 \times 10^{-3} cm^{-1}$. The line assignment and the fitting process in this work were performed by using XTDS as described above. From this analysis, we could find the anharmonic constants X_{33}, G_{33} and T_{33} and make a comparison with the values in the literature. These values are shown in Table 2. In this table, we also show the correspondence of symmetry species between the T_d and O_h groups. This correspondence allows us to express the vibrational anharmonic terms of $2\nu_3$ and $3\nu_3$ in the O_h group according to Hecht's expressions [25] that were developed for tetrahedral molecules. A general agreement is obtained, even though the differences are beyond the standard deviations indicated.

Equation (5) gives the general expression for vibrational terms of the vibrational energy which contains the anharmonic constants.

$$E_i^{vib} = \omega_i(v_i + \frac{d_i}{2}) + X_{ii}(v_i + \frac{d_i}{2})^2 + W(i, symmetry, G_{ii}, T_{ii}) \quad (5)$$

In this equation, ω_i gives the harmonic frequency, v_i the vibrational quantum number and the d_i represents the degeneracy of the normal mode. The W term gives the splitting contribution according to the symmetry of the sub-level. As for X_{ii}, G_{ii} and T_{ii} are anharmonic parameters of the vibrational level.

Table 2. In this table is shown: The correspondence of symmetry species between T_d and O_h groups, the values of X_{33}, G_{33} and T_{33} anharmonic constants. Vibrational expression terms and their values according to the symmetry of the sub-level are also shown.

Correspondence of symmetry species between T_d and O_h groups					
T_d	A_1	A_2	E	F_1	F_2
O_h	$A_{1g}+A_{2u}$	$A_{2g}+A_{1u}$	E_g+E_u	$F_{1g}+F_{2u}$	$F_{2g}+F_{1u}$
Comparison of derived anharmonicity constants.					
References	$\nu_3(cm^{-1})$		$X_{33}(cm^{-1})$	$G_{33}(cm^{-1})$	$T_{33}(cm^{-1})$
[7]			$-1.7456(5)$	0.924986(13)	$-0.248651(2)$
[6]	948.007500		-1.742565^a	0.918805(13)	$-0.246351(3)$
[24]			-1.680^a	0.861^a	-0.215^a
This work	948.102512(21)		$-1.7378(6)$	0.9122(8)	$-0.2498(1)$
Symmetry species	$(2\nu_3)$	Vibrational anharmonic terms		Values (cm^{-1})	
A_{1g}	$(2\nu_3)_{A1g}$	$= 2 \times \nu_3 + 2X_{33} - 2G_{33}$		1889.01 [7]	
E_g	$(2\nu_3)_{Eg}$	$= 2 \times \nu_3 + 2X_{33} + 6G_{33} + 12T_{33}$		1891.58 [7]	
F_{2g}	$(2\nu_3)_{F2g}$	$= 2 \times \nu_3 + 2X_{33} + 4G_{33} - 8T_{33}$		1896.68 [7]	
Symmetry species	$(3\nu_3)$	Vibrational anharmonic terms		Values (cm^{-1})	
A_{2u}	$(2\nu_3)_{A2u}$	$= 3 \times \nu_3 + 6X_{33} + 6G_{33} - 24T_{33}$		2845.3488	This work
F_{2u}	$(2\nu_3)_{F2u}$	$= 3 \times \nu_3 + 6X_{33} + 6G_{33} - 4T_{33}$		2840.3531	This work
F_{1u} $l = 3$	$(2\nu_3)_{F1u}$	$= 3 \times \nu_3 + 6X_{33} + G_{33} + 6T_{33} + [(5G_{33} + 6T_{33}) + 384T_{33}^2]^{1/2}$		8239.0432	This work
F_{1u} $l = 1$	$(2\nu_3)_{F1u}$	$= 3 \times \nu_3 + 6X_{33} + G_{33} + 6T_{33} - [(5G_{33} + 6T_{33}) + 384T_{33}^2]^{1/2}$		2827.5455	This work

[a] No stan viation given

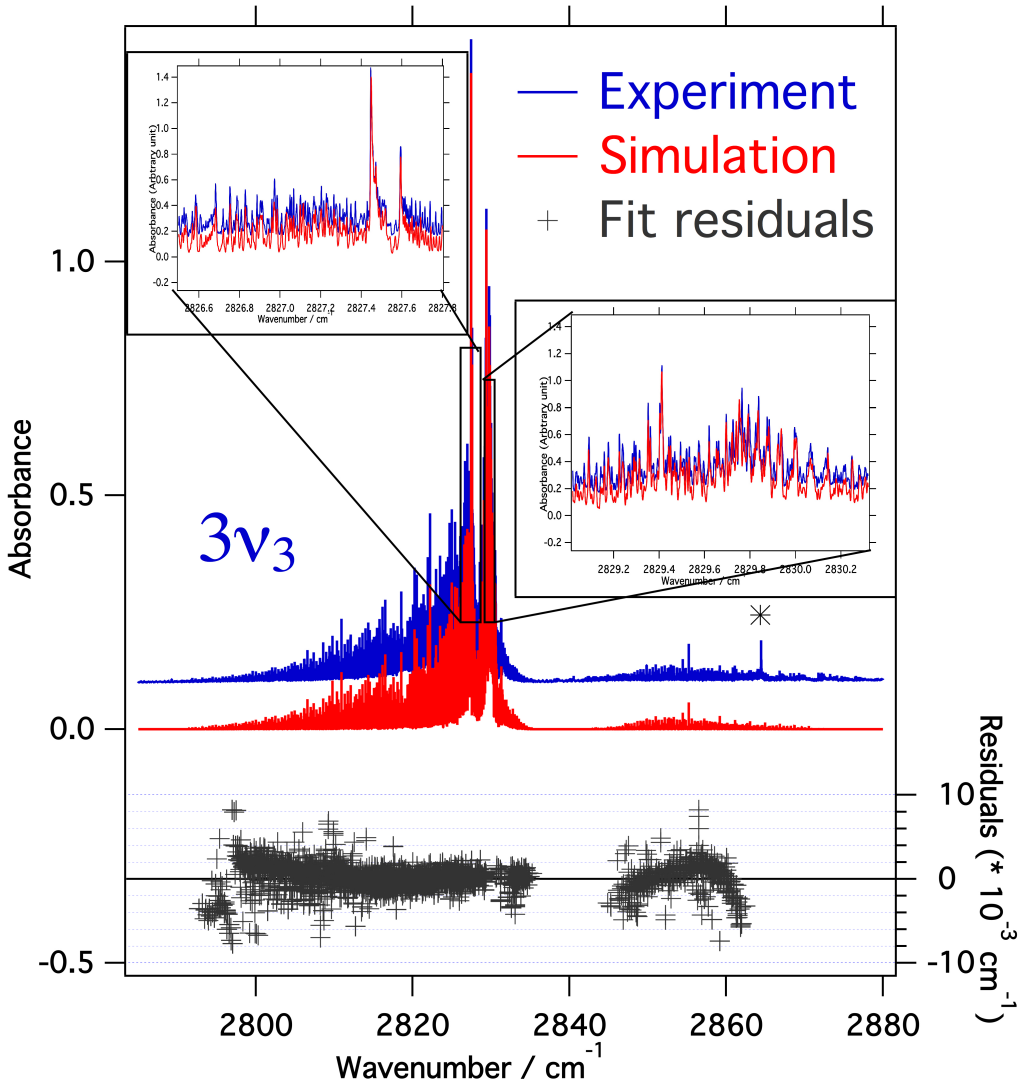

Figure 5. Comparison between the simulation(red) and the experiment (blue) spectrum recorded over the whole $3\nu_3$ band, showing the agreement achieved. The asterisk at 2864 cm^{-1} designates another weak transition which corresponds to $3\nu_2 + \nu_3$ according to [22].

9 Simultaneous fit of ν_1, ν_2, ν_3, $\nu_1 + \nu_3$, $\nu_2 + \nu_3$, $2\nu_3$, $\nu_1 + \nu_2 + \nu_3$, $3\nu_3$, $\nu_3 - \nu_1$, $\nu_3 - \nu_2$ data

SF_6 bands are usually studied as isolated bands by assuming that they do not interact with each other, but some interactions may exist between several bands and in turn have influences on the effective Hamiltonian parameters. To take into account such interactions and thus bring more coherence to the band analyses, we have achieved a global fit of 21102 lines of eleven bands implying the ν_1, ν_2 and ν_3 stretching modes. To make this global fit, we built a unique parameter file of all the ν_1, ν_2, ν_3, $\nu_1 + \nu_3$, $\nu_2 + \nu_3$, $2\nu_3$, $\nu_1 + \nu_2 + \nu_3$, $3\nu_3$, $\nu_3 - \nu_1$, $\nu_3 - \nu_2$ bands thanks to the HTDS software. In this analysis process, each level is represented by a polyad P_i (Table 3) and the bands by transitions between polyads (Table 4). Table 4 summarizes also the number of line positions fitted, the J_{max} values and the standard deviation corresponding to each band. The total number of fitted lines and the global standard deviation are also shown at the bottom of the table. To initiate the analysis, we took ν_1, ν_2, $2\nu_3$, $\nu_3 - \nu_1$ and $\nu_3 - \nu_2$ data from [31], while the ν_3, $\nu_1 + \nu_3$, $\nu_2 + \nu_3$, $\nu_1 + \nu_2 + \nu_3$ and $3\nu_3$ initial data are those obtained from the analysis in sections 5, 6, 7 and 8 presented above.

Table 3. Polyad representation of the energy levels

Polyads	P_0	P_1	P_2	P_3	P_4	P_5	P_6	P_7	P_8	P_9
Energy level	GS	v_2=1	v_1=1	v_3=1	v_1=2	v_2=v_3=1	v_1=v_3=1	v_3=2	v_1=v_2=v_3=1	v_3=3

Table 4. Summary of the global fit statistics:

Transitions		Bands	Assigned Frequency Data	J_{max} value	Standard Deviation (mk)
$P_1 \leftarrow P_0$	$\longrightarrow$	ν_2	543	58	2.713
$P_2 \leftarrow P_0$	$\longrightarrow$	ν_1	85	107	0.531
$P_3 \leftarrow P_0$	$\longrightarrow$	ν_3	1643	67	0.308
$P_5 \leftarrow P_0$	$\longrightarrow$	$\nu_2 + \nu_3$	3256	72	0.450
$P_6 \leftarrow P_0$	$\longrightarrow$	$\nu_1 + \nu_3$	1163	63	0.279
$P_7 \leftarrow P_0$	$\longrightarrow$	$2\nu_3$	128	59	0.057
$P_8 \leftarrow P_0$	$\longrightarrow$	$\nu_1 + \nu_2 + \nu_3$	2856	73	0.879
$P_9 \leftarrow P_0$	$\longrightarrow$	$3\nu_3$	3759	77	1.157
$P_3 \leftarrow P_1$	$\longrightarrow$	$\nu_3 - \nu_2$	6450	78	0.305
$P_3 \leftarrow P_2$	$\longrightarrow$	$\nu_3 - \nu_1$	987	79	0.365
$P_7 \leftarrow P_3$	$\longrightarrow$	$2\nu_3 - \nu_3$	232	59	0.003
Total number of fitted line positions: 21102; Global Standard deviation: 0.795					

10 Prediction of $\nu_1 + 3\nu_3$ and $\nu_2 + 3\nu_3$bands

After performing a global fit of data including the ν_1, ν_2, ν_3 $2\nu_3$ and $3\nu_3$, it becomes possible to predict multi quanta combinations between v_1=1, v_2=1, v_2=1, v_3=1, v_3=2 and v_3=3 levels. The only remaining concern is the small anharmonic shift coming from the neglect of higher order anharmonic terms.

To test the efficiency of our global model of the Hamiltonian parameters, predictions of $\nu_2 + 3\nu_3$ and $\nu_1 + 3\nu_3$ bands have been carried out, as shown in Fig. 6 and Fig. 7, respectively, after anharmonic shift correction (-0.274 cm^{-1} for $\nu_2 + 3\nu_3$ and -0.581 cm^{-1} for $\nu_1 + 3\nu_3$). We can see in these two predictions that the simulated spectra reproduce quite well the experimental spectra and thus may lead to assignments of the rovibrational lines.

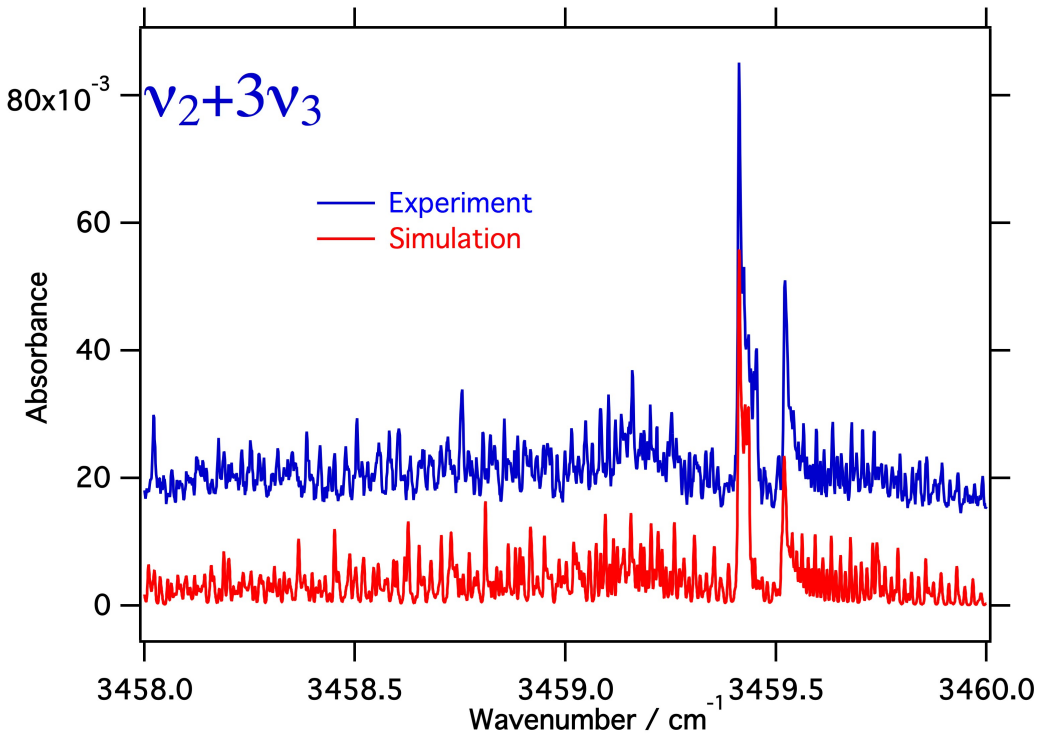

Figure 6. Comparison between an experimental spectrum (top curve, blue) (45 m optical path, 4.6 mb SF_6, T= 163 K) and a simulation (bottom, red curve) using the parameter of table 5 for $\nu_2 + 3\nu_3$ band. The experiment curve has been shifted for clarity.

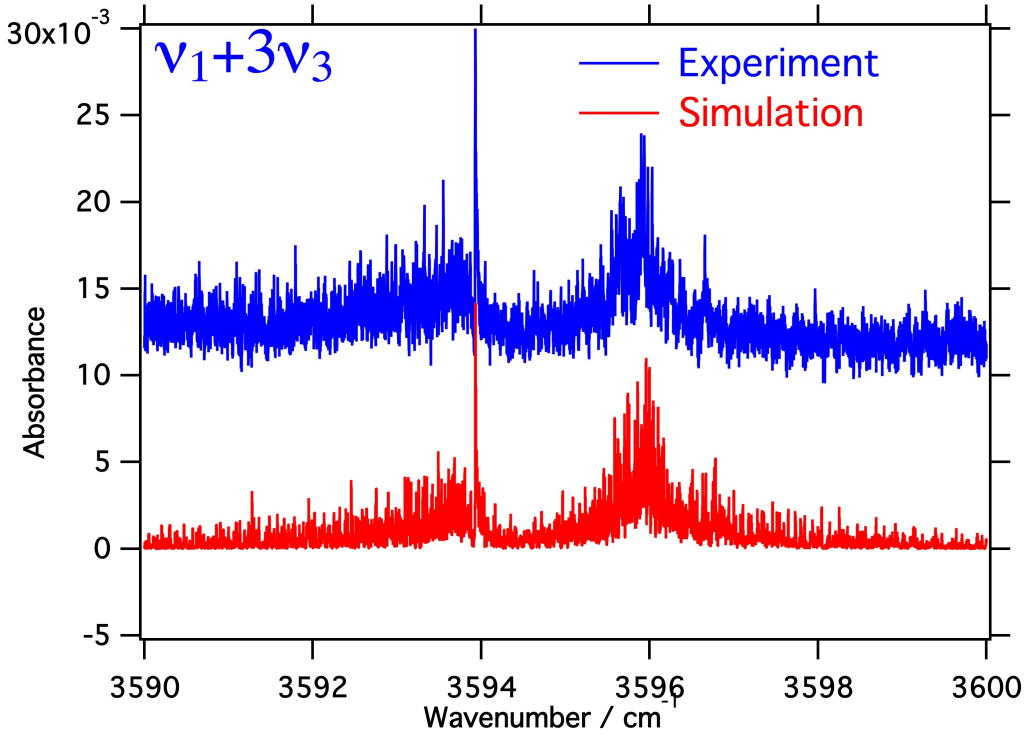

Figure 7. Comparison between an experimental spectrum (top curve, blue) (45 m optical path, 4.6 mb SF_6, T= 163 K) and a simulation (bottom, red curve) using the parameter in table 5 for $\nu_1 + 3\nu_3$ band. The experiment curve has been shifted for clarity.

11 Conclusion

Combining various experimental parameters (optical path, pressure, spectral range) using HR FTIR, synchrotron radiation and a long path cryogenic cell, we have measured a number of vibrational bands involving the stretching modes of SF_6 up to v_1, v_2=1, 2 and v_3=1 − 3. Using the tensorial formalism and the XTDS Dijon Software, a global fit of 11 rovibrationally resolved transitions has been carried out and a new optimized parameter set is proposed adding precision and global consistency for the interpretation of molecular spectroscopic parameters. It can also serve for the prediction of vibrational transitions up to four vibrational quanta, with description of the rotational structure. This model can serve as a basis for an extension to other multi quanta transitions of SF_6 or other octahedral molecules of technological relevance.

Acknowledgments

We gratefully acknowledge the support from the DIM-Analytics program of the Ile de France Region and the LEFE-CHAT program of CNRS.

References

[1] C Schwab, A.J Damiao, C.A.B Silveira, J.W. Neri, M.G Destro, M.G Rodrigues, N.A.S Riva, *Progress in Nuclear Energy* **33 (1-2)**, 217 (1998).
[2] W Eerkens, B.J Kim, *American Institute of Chemical Engineers (AiChE) Journal* **56 (9)**, 2331 (2010).
[3] C.D Cantrell, A.A. Letokov, A.A. Makarov, *Eds. Springer, Berlin* , 3232 (1980)
[4] J.L Lyman, G.P. Quigley, O.P. Judd, *Eds. Springer, Berlin* , 3232 (1979)
[5] A.S. Pine, A.G. Robiette, *J. Mol. Spectrosc.* **80**, 388 (1980).

[6] C. Patterson, B.J. Krohn, A.S. Pine, *J. Mol. Spectrosc.* **88**, 133 (1981).
[7] C. Patterson, F. Herlemont, M. Azizi, J. Lemaire, *J. Mol. Spectrosc.* **108**, 31 (1984).
[8] C. Chapados, G. Birnbaum, *J. Mol. Spectrosc.* **132**, 323 (1988).
[9] B. Bobin, C. Bord, J. Bord, C. Brant, *J. Mol. Spectrosc.* **121**, 91 (1987).
[10] V. Boudon, and J.-P.Champion, T. Gabard, M. Loëte, F. Michelot, G. Pierre, M. Rotger, C. Wenger, M. Rey, *J. Mol. Spectrosc.* **251**, 102 (2004), ISSN 0022-2852.
[11] O. Acef, C. Bordé, A. Clairon, G. Pierre, B. Sartakov, *J. Mol. Spectrosc.* **199**, 188 (2000).
[12] V. Boudon, H. Bürger, E.B. M'Kami, *J. Mol. Spectrosc.* **205**, 304 (2001).
[13] D. Bermejo, R.Z. Martinez, E. Loubignac, G. Pierre, *J. Mol. Spectrosc.* **201**, 164 (2000).
[14] V. Boudon, D. Bermejo, *J. Mol. Spectrosc.* **213**, 139 (2002).
[15] V. Boudon, J.L. Domenech, D Bermejo, H. Willner, *J. Mol. Spectrosc.* **228**, 392 (2004).
[16] V. Boudon, L. Manceron, F. Kwabia Tchana, M. Loëte, L. Lago, P. Roy, *Phys. Chem. Chem. Phys.* **16**, 1415 (2014).
[17] B. D. Hall, G. S. Dutton, D. J. Mondeel, J. D. Nance, M. Rigby, J. H. Butler, F. L. Moore, D. F. Hurst, J. W. Elkins, *Atmos. Meas. Tech.* **4**, 2441-2451 (2011).
[18] V. Chin, L. Person, *J. Mol. Spectrosc.* **98**, 258 (1983).
[19] W. Person, B. J. Krohn, *J. Mol. Spectrosc.* **98**, 229 (1983).
[20] R. S. Mc Dowell, B. J. Krohn, H. Fliker, M. C. Vasquez, *Spectrochim. Acta* **42 A**, 351 (1986).
[21] R. S. Mc Dowell, B. J. Krohn, *Spectrochim. Acta* **42 A**, 371 (1986).
[22] H. Levene, D. S. Perry, *J. Chem. Phys.* **80(5)**, 1772 (1984).
[23] D. P. Hodgkinson, R. K. Heenan, A. R. Hoy, A. G. Robiette, *Mol. Phys.* **48**, 193 (1984).
[24] D. P. Hodgkinson, J. C. Barrette, A. G. Robiette, *Mol. Phys.* **54**, 927 (1985).
[25] K. T. Hetch, *J. Mol. Spectrosc.* **5**, 355-389 (1960).
[26] J. Zhang, Q. Zhong, N. Wu, J. Wang, J. Zhao, Y. Xu, S. Guo, C. Ying, *Phys. Lett. A* **215**, 291 (1996).
[27] P. Roy, J.B. Brubach, M. Rouzires, O. Pirali, L. Manceron, F. Kwabia Tchana, *Rev. Electricité et Electronique* **2**, 23 (2008).
[28] J.B. Brubach, L. Manceron, M. Rouzires, O. Pirali, D. Balcon, F. Kwabia Tchana, V. Boudon, M. Tudorie, T. Huet, A. Cuisset, P. Roy, *Infrared Physics and Technology* , 112 (2009).
[29] F. K. Tchana, F. Willaert, X. Landsheere, J. - M. Flaud, L. Lago, M. Chapuis, P. Roy, L. Manceron, *Rev. Sci. Inst.* **84**, 093101 (2013).
[30] M. Faye,, M. Bordessoule, B. Kanouté, P. Roy, L. Manceron, Rev. Sci. Inst. **87** 063119 2016.
[31] M. Faye, A. Leven, V. Boudon, L. Manceron, P. Asselin, F. Kwabia Tchana, P. Roy, *Mol. Phys.* **909059**, 112 (2014).
[32] S. te Lintel. Hekkert, and A. F.Linskens, B. G Sartakov, G. Pierre, J. Reuss, *J. Chem. Phys.* **177**, 181 (1993).
[33] M. Kelkhal, E. Rusinek, J. Legrand, F. Herlemont, and G.Pierre, *J. Chem. Phys.* **107(15)**, 5694 (1997).
[34] L.S. Rothman,, D. Jacquemart, A Barbe, D.C. Benner, M Birk, L.R. Brown, M.R. Carleer, C. Chackerian, K. Chance, L. Coudert, V. Dana, V. Malathy-Devi, J. M. Flaud, R. R. Gamache, A. Goldman, J.M. Hartmann, K.W. Jucks, A.G. Maki, J.Y. Mandin, S. Massie, J. Orphal, A. Perrin, C.P. Rinsland, M.A. Smith, R.A. Toth, J. Vander Auwera, P. Varanasi, G. Wagner, *J. Quant. Spectrosc. Rad. Trans.* **96** 139 2005.
[35] J. R. Ackerhalt, H. Fliker, H. W. Galbraith, J. King, and W. B. Person, *J. Chem. Phys.* **69**, 1461 (1978).
[36] A. Robiette, D. Gray, F. Birss, *Mol. Phys.* **32 (6)**, 1591-1607 (1976).

APPENDIX

In this Appendix section we summarize in table 5, the effective Hamiltonian parameters resulting from the global fit presented above.

The ground state parameter values are fixed to

Table 5. Effective Hamiltonian parameters. Standard deviation is given in parentheses, in the unit of the last two digits. Parameters for which no standard is given are fixed to literature value.

Bande	Order	$\Omega(K,n\Gamma)$	Paramètres {s}	{s'}	Values / cm^{-1}(St.Dev.)	"Usual" notation, [36] and comments.
GS	0	$2(0,0A_{1g})$	$000000A_{1g}$	$000000A_{1g}$	$9.1075666449 \times 10^{-2}$ ‡	B_0
	2	$4(0,0A_{1g})$	$000000A_{1g}$	$000000A_{1g}$	$-7.2689461558 \times 10^{-9}$‡	$-D_0$
	2	$4(4,0A_{1g})$	$000000A_{1g}$	$000000A_{1g}$	$1.2227986553 \times 10^{-10}$‡	$-(\sqrt{15}/4\sqrt{2})D_{0t}$
	4	$6(0,0A_{1g})$	$000000A_{1g}$	$000000A_{1g}$	$2.3994500822 \times 10^{-13}$‡	H_0
	4	$6(4,0A_{1g})$	$000000A_{1g}$	$000000A_{1g}$	$6.2051155575 \times 10^{-16}$‡	$(3\sqrt{5}/16\sqrt{2})H_{4t}$
	4	$6(6,0A_{1g})$	$000000A_{1g}$	$000000A_{1g}$	$1.7088642943 \times 10^{-15}$‡	$-(\sqrt{231}/64\sqrt{2})H_{4t}$
	6	$8(0,0A_{1g})$	$000000A_{1g}$	$000000A_{1g}$	$-2.3273163437 \times 10^{-17}$‡	L_0
	6	$8(4,0A_{1g})$	$000000A_{1g}$	$000000A_{1g}$	$1.6814688738 \times 10^{-19}$‡	$-(3\sqrt{15}/64\sqrt{2})L_{4t}$
	6	$8(6,0A_{1g})$	$000000A_{1g}$	$000000A_{1g}$	$2.4028125090 \times 10^{-19}$‡	$(3\sqrt{77}/256\sqrt{2})L_{6t}$
	6	$8(8,0A_{1g})$	$000000A_{1g}$	$000000A_{1g}$	$4.4485213255 \times 10^{-20}$‡	$(1/32\sqrt{33})L_{8t}$
ν_2	0	$0(0,0A_{1g})$	$010000E_g$	$010000E_g$	643.373626(43)	ν_2
	2	$2(0,0A_{1g})$	$010000E_g$	$010000E_g$	$1.9089(70) \times 10^{-5}$	$B_2 - B_0$
	2	$2(2,0E_g\ )$	$010000E_g$	$010000E_g$	$3.4144(45) \times 10^{-5}$	$\sqrt{3}b_2 + (24\sqrt{3}/7)C_6$
	3	$3(3,0A_{2g})$	$010000E_g$	$010000E_g$	$-1.350(51) \times 10^{-8}$	$(1/2)d_2$
	4	$4(0,0A_{1g})$	$010000E_g$	$010000E_g$	$-5.49(34) \times 10^{-10}$	$-(D_2 - D_0)$
	4	$4(2,0E_g\ )$	$010000E_g$	$010000E_g$	$1.13(13) \times 10^{-10}$	
	4	$4(4,0A_{1g})$	$010000E_g$	$010000E_g$	$-1.62(33) \times 10^{-11}$	
	4	$4(4,0E_g\ )$	$010000E_g$	$010000E_g$	$2.42(71) \times 10^{-11}$	
	5	$5(3,0A_{2g})$	$010000E_g$	$010000E_g$	$1.75(59) \times 10^{-13}$	
	6	$6(0,0A_{1g})$	$010000E_g$	$010000E_g$	$1.64(48) \times 10^{-14}$	
	6	$6(2,0E_g\ )$	$010000E_g$	$010000E_g$	$-6.52(90) \times 10^{-15}$	
	6	$6(4,0A_{1g})$	$010000E_g$	$010000E_g$	$1.73(36) \times 10^{-15}$	
	6	$6(4,0E_g\ )$	$010000E_g$	$010000E_g$	$2.71(79) \times 10^{-15}$	
ν_1	0	$0(0,0A_{1g})$	$100000A_{1g}$	$100000A_{1g}$	774.545540(66)	ν_1
	2	$2(0,0A_{1g})$	$100000A_{1g}$	$100000A_{1g}$	$-1.10712(47)) \times 10^{-4}$	$B_1 - B_0$
	4	$4(0,0A_{1g})$	$100000A_{1g}$	$100000A_{1g}$	$3.00(68) \times 10^{-11}$	$-(D_1 - D_0)$
	4	$4(4,0A_{1g})$	$100000A_{1g}$	$100000A_{1g}$	$6.4(1.2) \times 10^{-12}$	
ν_3	0	$0(0,0A_{1g})$	$001000F_{1u}$	$001000F_{1u}$	948.1025121(21)	ν_3
	1	$1(1,0F_{1g})$	$001000F_{1u}$	$001000F_{1u}$	$2.6754759(88) \times 10^{-1}$	$3\sqrt{2}(B\zeta)_3$ ν_3 (Coriolis)
	2	$2(0,0A_{1g})$	$001000F_{1u}$	$001000F_{1u}$	$-1.310341(89) \times 10^{-4}$	$B_3 - B_0$
	2	$2(2,0E_g)$	$001000F_{1u}$	$001000F_{1u}$	$-1.58495(16) \times 10^{-4}$	$-(1/2)\alpha^3_{220} - 6\alpha^3_{224}$
	2	$2(2,0F_{2g})$	$001000F_{1u}$	$001000F_{1u}$	$4.3836(16) \times 10^{-5}$	$-(3/4)\alpha^3_{220} + 6\alpha^3_{224}$
	3	$3(1,0F_{1g})$	$001000F_{1u}$	$001000F_{1u}$	$3.208(54) \times 10^{-8}$	$-(3\sqrt{3}/4\sqrt{2})F^3_{110}$
	3	$3(3,0F_{1g})$	$001000F_{1u}$	$001000F_{1u}$	$-7.7(4.1) \times 10^{-10}$	$(3/\sqrt{5}/2)F^3_{134}$
	4	$4(0,0A_{1g})$	$001000F_{1u}$	$001000F_{1u}$	$-7.67(65) \times 10^{-11}$	$-(D_3 - D_0)$
	4	$4(2,0E_g\ )$	$001000F_{1u}$	$001000F_{1u}$	$-2.40(43) \times 10^{-10}$	
	4	$4(2,0F_{2g})$	$001000F_{1u}$	$001000F_{1u}$	$2.77(44) \times 10^{-10}$	
	4	$4(4,0A_{1g})$	$001000F_{1u}$	$001000F_{1u}$	$2.0(2.1) \times 10^{-12}$	
	4	$4(4,0E_g\ )$	$001000F_{1u}$	$001000F_{1u}$	$3.61(67) \times 10^{-10}$	
	4	$4(4,0F_{2g})$	$001000F_{1u}$	$001000F_{1u}$	$2.64(51) \times 10^{-10}$	
	5	$5(1,0F_{1g})$	$001000F_{1u}$	$001000F_{1u}$	$-3.2(1.0) \times 10^{-13}$	
	5	$5(3,0F_{1g})$	$001000F_{1u}$	$001000F_{1u}$	$2.71(37) \times 10^{-12}$	
	5	$5(5,0F_{1g})$	$001000F_{1u}$	$001000F_{1u}$	$2.52(39) \times 10^{-12}$	
	5	$5(5,1F_{1g})$	$001000F_{1u}$	$001000F_{1u}$	$0.998(93) \times 10^{-12}$	
	6	$6(0,0A_{1g})$	$001000F_{1u}$	$001000F_{1u}$	$1.6(1.3) \times 10^{-15}$	
	6	$6(2,0E_g\ )$	$001000F_{1u}$	$001000F_{1u}$	$-3.4226181004 \times 10^{-15}$†	
	6	$6(2,0F_{2g})$	$001000F_{1u}$	$001000F_{1u}$	$1.13(69) \times 10^{-15}$	
	6	$6(4,0A_{1g})$	$001000F_{1u}$	$001000F_{1u}$	$1.06(18) \times 10^{-15}$	
	6	$6(4,0E_g\ )$	$001000F_{1u}$	$001000F_{1u}$	$6.74(83) \times 10^{-15}$	
	6	$6(4,0F_{2g})$	$001000F_{1u}$	$001000F_{1u}$	$-5.08(38) \times 10^{-14}$	
	6	$6(6,0A_{1g})$	$001000F_{1u}$	$001000F_{1u}$	$-5.23(64) \times 10^{-16}$	
	6	$6(6,0E_g\ )$	$001000F_{1u}$	$001000F_{1u}$	$-5.37(45) \times 10^{-15}$	
	6	$6(6,0F_{2g})$	$001000F_{1u}$	$001000F_{1u}$	$-6.77(48) \times 10^{-14}$	
	6	$6(6,1F_{2g})$	$001000F_{1u}$	$001000F_{1u}$	$-1.5644920019 \times 10^{-15}$†	
	7	$7(1,0F_{1g})$	$001000F_{1u}$	$001000F_{1u}$	$-2.39(56) \times 10^{-17}$	
	7	$7(3,0F_{1g})$	$001000F_{1u}$	$001000F_{1u}$	$3.4(1.0) \times 10^{-17}$	
	7	$7(5,0F_{1g})$	$001000F_{1u}$	$001000F_{1u}$	$2.04(74) \times 10^{-17}$	
	7	$7(5,1F_{1g})$	$001000F_{1u}$	$001000F_{1u}$	$3.29(62) \times 10^{-17}$	
	7	$7(7,0F_{1g})$	$001000F_{1u}$	$001000F_{1u}$	$1.6(1.8) \times 10^{-18}$	
	7	$7(7,1F_{1g})$	$001000F_{1u}$	$001000F_{1u}$	$6.6(5.0) \times 10^{-18}$	
$\nu_2 + \nu_3$	2	$0(0,0A_{1g})$	$011000F_{1u}$	$011000F_{1u}$	$-3.759037(85)$	F_{1u} Sublevel
	3	$1(1,0F_{1g})$	$011000F_{1u}$	$011000F_{1u}$	$5.0043(58) \times 10^{-3}$	F_{1u} Coriolis
	4	$2(0,0A_{1g})$	$011000F_{1u}$	$011000F_{1u}$	$2.228(13) \times 10^{-5}$	
	4	$2(2,0E_g\ )$	$011000F_{1u}$	$011000F_{1u}$	$1.3648(89) \times 10^{-5}$	
	4	$2(2,0F_{2g})$	$011000F_{1u}$	$011000F_{1u}$	$-3.318(16) \times 10^{-5}$	
	5	$3(1,0F_{1g})$	$011000F_{1u}$	$011000F_{1u}$	$4.06(42) \times 10^{-8}$	
	5	$3(3,0F_{1g})$	$011000F_{1u}$	$011000F_{1u}$	$1.032(34) \times 10^{-7}$	
	3	$1(1,0F_{1g})$	$011000F_{1u}$	$011000F_{2u}$	$-3.9093138624 \times 10^{-4}$†	$F_{1u} - F_{1u}$ Interaction
	4	$2(2,0E_g\ )$	$011000F_{1u}$	$011000F_{2u}$	$-2.5563(85) \times 10^{10-5}$	
	4	$2(2,0F_{2g})$	$011000F_{1u}$	$011000F_{2u}$	$-3.52(25) \times 10^{-6}$	
	5	$3(1,0F_{1g})$	$011000F_{1u}$	$011000F_{2u}$	$-1.15(13) \times 10^{-8}$	
	2	$0(0,0A_{1g})$	$011000F_{2u}$	$011000F_{2u}$	$-2.8537(19) \times 10^{-1}$	F_{2u} Sublevel
	3	$1(1,0F_{1g})$	$011000F_{2u}$	$011000F_{2u}$	$2.761(12) \times 10^{-3}$	F_{2u} Coriolis
	4	$2(0,0A_{1g})$	$011000F_{2u}$	$011000F_{2u}$	$-3.203(20) \times 10^{-5}$	
	4	$2(2,0E_g\ )$	$011000F_{2u}$	$011000F_{2u}$	$-2.498(17) \times 10^{-5}$	
	4	$2(2,0F_{2g})$	$011000F_{2u}$	$011000F_{2u}$	$2.380(21) \times 10^{-5}$	
	5	$3(1,0F_{1g})$	$011000F_{2u}$	$011000F_{2u}$	$-9.41(46) \times 10^{-8}$	
	5	$3(3,0F_{1g})$	$011000F_{2u}$	$011000F_{2u}$	$-5.85(44) \times 10^{-8}$	

Bande	Order	$\Omega(K, n\Gamma)$	Paramètres {s}	{s'}	Values / cm^{-1}(St.Dev.)	"Usual" notation
$2\nu_1$	2	$0(0,0A_{1g})$	$200000A_{1g}$	$200000A_{1g}$	-1.7346356396	Anharmonicit $2X_{11}$
	4	$2(0,0A_{1g})$	$200000A_{1g}$	$200000A_{1g}$	$-1.2576597821 \times 10^{-5}$	ΔB_{11}
	6	$4(0,0A_{1g})$	$200000A_{1g}$	$200000A_{1g}$	$-4.9546135312 \times 10^{-9}$	$-\Delta D_{11}$
	6	$4(4,0A_{1g})$	$200000A_{1g}$	$200000A_{1g}$	$-7.7163949322 \times 10^{-11}$	$-(\sqrt{15}/4\sqrt{2})D_{11t}$
$\nu_1 + \nu_3$	2	$0(0,0A_{1g})$	$101000F_{1u}$	$101000F_{1u}$	-2.908879(81)	Anharmonicit X_{13}
	3	$1(1,0F_{1g})$	$101000F_{1u}$	$101000F_{1u}$	$-7.91(22) \times 10^{-5}$	Coriolis
	4	$2(0,0A_{1g})$	$101000F_{1u}$	$101000F_{1u}$	$-7.1(4.8) \times 10^{-8}$	
	4	$2(2,0E_g)$	$101000F_{1u}$	$101000F_{1u}$	$2.976(71) \times 10^{-6}$	
$\nu_1 + \nu_2 + \nu_3$	4	$0(0,0A_{1g})$	$111000F_{1u}$	$111000F_{1u}$	$-2.39186(13)$	F_{1u} Sublevel
	5	$1(1,0F_{1g})$	$111000F_{1u}$	$111000F_{1u}$	$8.42(20) \times 10^{-4}$	
	6	$2(0,0A_{1g})$	$111000F_{1u}$	$111000F_{1u}$	$3.100(96) \times 10^{-4}$	
	6	$2(2,0E_g)$	$111000F_{1u}$	$111000F_{1u}$	$2.351(72) \times 10^{-4}$	
	6	$2(2,0F_{2g})$	$111000F_{1u}$	$111000F_{1u}$	$-3.46(11) \times 10^{-4}$	
	7	$3(1,0F_{1g})$	$111000F_{1u}$	$111000F_{1u}$	$-1.52(15) \times 10^{-7}$	
	7	$3(3,0F_{1g})$	$111000F_{1u}$	$111000F_{1u}$	$1.60(18) \times 10^{-7}$	
	5	$1(1,0F_{1g})$	$111000F_{1u}$	$111000F_{2u}$	$-1.500(45) \times 10^{-2}$	$F_{1u} - F_{1u}$ interaction
	6	$2(2,0E_g)$	$111000F_{1u}$	$111000F_{2u}$	$-2.221(67) \times 10^{-4}$	
	6	$2(2,0F_{2g})$	$111000F_{1u}$	$111000F_{2u}$	$-7.39(42) \times 10^{-6}$	
	7	$3(1,0F_{1g})$	$111000F_{1u}$	$111000F_{2u}$	$-1.048(58) \times 10^{-6}$	
	7	$3(3,0A_{2g})$	$111000F_{1u}$	$111000F_{2u}$	$-1.93(11) \times 10^{-7}$	
	7	$3(3,0F_{1g})$	$111000F_{1u}$	$111000F_{2u}$	$7.04(24) \times 10^{-8}$	
	7	$3(3,0F_{2g})$	$111000F_{1u}$	$111000F_{2u}$	$-3.42(12) \times 10^{-7}$	
	4	$0(0,0A_{1g})$	$111000F_{2u}$	$111000F_{2u}$	$-2.48157(26)$	F_{2u} Sublevel
	5	$1(1,0F_{1g})$	$111000F_{2u}$	$111000F_{2u}$	$-2.855(24) \times 10^{-3}$	
	6	$2(0,0A_{1g})$	$111000F_{2u}$	$111000F_{2u}$	$-2.982(95) \times 10^{-4}$	
	6	$2(2,0E_g)$	$111000F_{2u}$	$111000F_{2u}$	$-2.143(72) \times 10^{-4}$	
	6	$2(2,0F_{2g})$	$111000F_{2u}$	$111000F_{2u}$	$3.41(11) \times 10^{-4}$	
	7	$3(1,0F_{1g})$	$111000F_{2u}$	$111000F_{2u}$	$-1.00(14) \times 10^{-7}$	
	7	$3(3,0F_{1g})$	$111000F_{2u}$	$111000F_{2u}$	$2.28(18) \times 10^{-7}$	
$2\nu_3$	2	$0(0,0A_{1g})$	$002000A_{1g}$	$002000A_{1g}$	$-7.195264(72)$	$A_{1g} = 2X_{33} - 2G_{33}$
	4	$2(0,0A_{1g})$	$002000A_{1g}$	$002000A_{1g}$	$2.003(72) \times 10^{-6}$	
	6	$4(0,0A_{1g})$	$002000A_{1g}$	$002000A_{1g}$	$1.95(17) \times 10^{-10}$	
	6	$4(4,0A_{1g})$	$002000A_{1g}$	$002000A_{1g}$	$5.70(25) \times 10^{-11}$	
	4	$2(2,0E_g)$	$002000A_{1g}$	$002000E_g$	$-7.99(57) \times 10^{-7}$	
	6	$4(2,0E_g)$	$002000A_{1g}$	$002000E_g$	$-7.13(95) \times 10^{-11}$	
	6	$4(4,0E_g)$	$002000A_{1g}$	$002000E_g$	$1.43(14) \times 10^{-10}$	
	4	$2(2,0F_{2g})$	$002000A_{1g}$	$002000F_{2g}$	$-2.72(26) \times 10^{-6}$	
	5	$3(3,0F_{2g})$	$002000A_{1g}$	$002000F_{2g}$	$-4.04(79) \times 10^{-8}$	
	6	$4(2,0F_{2g})$	$002000A_{1g}$	$002000F_{2g}$	$-1.90(25) \times 10^{-10}$	
	6	$4(4,0F_{2g})$	$002000A_{1g}$	$002000F_{2g}$	$-9.8(1.6) \times 10^{-11}$	
	2	$0(0,0A_{1g})$	$002000E_g$	$002000E_g$	$-4.630220(24)$	$E_g = 2X_{33} + 6G_{33} + 12T_{33}$
	4	$2(0,0A_{1g})$	$002000E_g$	$002000E_g$	$-1.379(11) \times 10^{-4}$	
	4	$2(2,0E_g)$	$002000E_g$	$002000E_g$	$-1.1931(98) \times 10^{-4}$	
	5	$3(3,0A_{2g})$	$002000E_g$	$002000E_g$	$6.0(1.9) \times 10^{-9}$	
	6	$4(0,0A_{1g})$	$002000E_g$	$002000E_g$	$3.528(70) \times 10^{-9}$	
	6	$4(2,0E_g)$	$002000E_g$	$002000E_g$	$-1.681(28) \times 10^{-9}$	
	6	$4(4,0A_{1g})$	$002000E_g$	$002000E_g$	$3.4708425825 \times 10^{-11}$	
	6	$4(4,0E_g)$	$002000E_g$	$002000E_g$	$2.98(25) \times 10^{-10}$	
	3	$1(1,0F_{1g})$	$002000E_g$	$002000F_{2g}$	$-4.884(34) \times 10^{-3}$	
	4	$2(2,0F_{2g})$	$002000E_g$	$002000F_{2g}$	$6.319(54) \times 10^{-5}$	
	5	$3(1,0F_{1g})$	$002000E_g$	$002000F_{2g}$	$3.69(13) \times 10^{-8}$	
	5	$3(3,0F_{1g})$	$002000E_g$	$002000F_{2g}$	$-4.01(13) \times 10^{-8}$	
	5	$3(3,0F_{2g})$	$002000E_g$	$002000F_{2g}$	$2.34(36) \times 10^{-8}$	
	6	$4(2,0F_{2g})$	$002000E_g$	$002000F_{2g}$	$1.438(30) \times 10^{-9}$	
	6	$4(4,0F_{1g})$	$002000E_g$	$002000F_{2g}$	$2.87(49) \times 10^{-10}$	
	6	$4(4,0F_{2g})$	$002000E_g$	$002000F_{2g}$	$9.42(29) \times 10^{-10}$	
	2	$0(0,0A_{1g})$	$002000F_{2g}$	$002000F_{2g}$	$3.489013(37) \times 10^{-1}$	$F_{2g} = 2X_{33} + 4G_{33} - 8T_{33}$
	3	$1(1,0F_{1g})$	$002000F_{2g}$	$002000F_{2g}$	$5.460(20) \times 10^{-4}$	
	4	$2(0,0A_{1g})$	$002000F_{2g}$	$002000F_{2g}$	$8.895(77) \times 10^{-5}$	
	4	$2(2,0E_g)$	$002000F_{2g}$	$002000F_{2g}$	$-1.352(12) \times 10^{-4}$	
	4	$2(2,0F_{2g})$	$002000F_{2g}$	$002000F_{2g}$	$1.0343(87) \times 10^{-4}$	
	5	$3(1,0F_{1g})$	$002000F_{2g}$	$002000F_{2g}$	$-2.40(29) \times 10^{-8}$	
	5	$3(3,0F_{1g})$	$002000F_{2g}$	$002000F_{2g}$	$-2.07(26) \times 10^{-8}$	
	6	$4(0,0A_{1g})$	$002000F_{2g}$	$002000F_{2g}$	$-3.056(55) \times 10^{-9}$	
	6	$4(2,0E_g)$	$002000F_{2g}$	$002000F_{2g}$	$-2.728(42) \times 10^{-9}$	
	6	$4(2,0F_{2g})$	$002000F_{2g}$	$002000F_{2g}$	$2.535(46) \times 10^{-9}$	
	6	$4(4,0A_{1g})$	$002000F_{2g}$	$002000F_{2g}$	$-1.074(44) \times 10^{-10}$	
	6	$4(4,0E_g)$	$002000F_{2g}$	$002000F_{2g}$	$7.93(30) \times 10^{-10}$	
	6	$4(4,0F_{2g})$	$002000F_{2g}$	$002000F_{2g}$	$1.346(46) \times 10^{-9}$	

Bande	Order	$\Omega(K, n\Gamma)$	Paramètres {s}	{s'}	Values / cm^{-1}(St.Dev)	"Usual" notation
$3\nu_3$	4	$0(0,0A_{1g})$	$003000F_{1u}$	$003000F_{1u}$	$-1.981(22) \times 10^{-1}$	Sous niveau $F_{1u}^{(l_3)=1}$
	5	$1(1,0F_{1g})$	$003000F_{1u}$	$003000F_{1u}$	$-9.102(88) \times 10^{-3}$	F_{1u} Coriolis
	6	$2(0,0A_{1g})$	$003000F_{1u}$	$003000F_{1u}$	$-4.07(18) \times 10^{-6}$	
	4	$0(0,0A_{1g})$	$003000F_{1u}$	$003000F_{1u}$	$-2.218(16) \times 10^{-1}$	Interaction $F_{1u}^{(l_3)=1} - F_{1u}^{(l_3)=3}$
	5	$1(1,0F_{1g})$	$003000F_{1u}$	$003000F_{1u}$	$6.481(56) \times 10^{-3}$	
	6	$2(0,0A_{1g})$	$003000F_{1u}$	$003000F_{1u}$	$-8.1(2.8) \times 10^{-7}$	
	4	$0(0,0A_{1g})$	$003000A_{2u}$	$003000A_{2u}$	$-3.01(11) \times 10^{-2}$	Sous niveau A_{2u}
	6	$2(0,0A_{1g})$	$003000A_{2u}$	$003000A_{2u}$	$-9.2(7.4) \times 10^{-7}$	
	4	$0(0,0A_{1g})$	$003000F_{1u}$	$003000F_{1u}$	$2.633(22) \times 10^{-1}$	Sous niveau $F_{1u}^{(l_3)=3}$
	5	$1(1,0F_{1g})$	$003000F_{1u}$	$003000F_{1u}$	$3.413(36) \times 10^{-3}$	
	6	$2(0,0A_{1g})$	$003000F_{1u}$	$003000F_{1u}$	$5.41(25) \times 10^{-6}$	
	4	$0(0,0A_{1g})$	$003000F_{2u}$	$003000F_{2u}$	$-2.634(63) \times 10^{-2}$	Sous niveau F_{2u}
	5	$1(1,0F_{1g})$	$003000F_{2u}$	$003000F_{2u}$	$5.882(61) \times 10^{-3}$	
	6	$2(0,0A_{1g})$	$003000F_{2u}$	$003000F_{2u}$	$-3.42(35) \times 10^{-6}$	

‡ GS parameters are assumed enough good to be fixed in the fit.

† Parameters fixed to their initial values taken from a preliminary fit including less data.